EUROfusion

EUROFUSION CP(15)04/31

A. Hakola et al.

Gross and Net Erosion of Tungsten in the Outer Strike-Point Region of ASDEX Upgrade

(18th May 2015 – 22nd May 2015)
Aix-en-Provence, France

This work has been carried out within the framework of the EUROfusion Consortium and has received funding from the Euratom research and training programme 2014-2018 under grant agreement No 633053. The views and opinions expressed herein do not necessarily reflect those of the European Commission.

Gross and net erosion of tungsten in the outer strike-point region of ASDEX Upgrade

A Hakola[1], M I Airila[1], J Karhunen[2], M Groth[2], A Herrmann[3], K Krieger[3], T Kurki-Suonio[2], G Meisl[3], M Oberkofler[3], R Neu[3,4], S Potzel[3], V Rohde[3] and the ASDEX Upgrade Team

[1]VTT, P O Box 1000, 02044 VTT, Finland
[2]Aalto University, Department of Applied Physics, P O Box 14100, 00076 Aalto, Finland
[3]Max-Planck-Institut für Plasmaphysik, Boltzmannstrasse 2, 85748 Garching, Germany
[4]Technische Universität München, Boltzmannstrasse 15, 85748 Garching, Germany

E-mail: antti.hakola@vtt.fi

Abstract. We have investigated net and gross erosion of W in the outer strike-point (OSP) region of ASDEX Upgrade with the help of marker probes during low-density/high-temperature L-mode discharges. *Post mortem* analyses indicate net-erosion rates of 0.04-0.13nm/s, with the highest rates measured close to the OSP. The results generally agree with earlier campaign-integrated data. Re-deposition was some 30-40% of gross erosion, which is lower than what has earlier been obtained spectroscopically (~50-60%), possibly due to the special plasma conditions of our experiment. Gross erosion was also estimated by passive emission spectroscopy, and around the OSP the results matched with *post mortem* data. However, the spectroscopic erosion profile in the poloidal direction was much steeper than the *post mortem* one. Preliminary ERO simulations have predicted net erosion of the same order of magnitude as experimental results but reproducing the poloidal erosion/re-deposition profiles requires further work.

PACS: 52.40.Hf, 52.55.Fa, 82.80.Yc

1. Introduction

In future fusion reactors, the lifetime of plasma-facing components (PFCs) may be severely restricted due to their erosion by plasma and impurity particles [1]. In addition, retention of plasma fuel in co-deposited layers on PFCs may result in safety limits for radioactive tritium inside the reactor vessel being exceeded after only a small number of plasma discharges [2]. With these issues in mind, several candidate materials for PFCs have been studied, and tungsten (W) has proven to be the best choice: it has low erosion yield by plasma bombardment and retention of hydrogen isotopes in it is small [3,4]. Therefore, establishing a concise picture on the erosion, re-deposition, and migration characteristics of W in fusion reactors have a high priority in the European fusion research programme [5].

An important research question is elucidating the balance between gross and net erosion of W during different plasma operations [5]. Gross erosion denotes the number of atoms primarily removed from a PFC while net erosion is obtained by subtracting from the gross erosion the number of particles re-deposited on the surface. Re-deposition can be significant: According to measurements in the ASDEX Upgrade (AUG), TEXTOR, and JET tokamaks ~50% of gross erosion under average plasma operations [6]. In high-density and low-temperature plasmas, re-deposition fractions even up to 90%

have been inferred [5]. In the case of W, a large fraction of the particles returning onto the surface are *promptly re-deposited*, i.e., the emitted W atoms are ionized in the plasma, within the distance of the Larmor radius from the surface, and immediately deposited back on the PFC during their first gyro orbit [4].

Here, we have studied net and gross erosion as well as prompt re-deposition of W in the outer strike point (OSP) region of AUG; in this region, both erosion and re-deposition are known to play the largest roles. The results have been extracted from *post mortem* measurements of special marker probes, exposed to low-density/high-temperature L-mode plasma discharges in AUG using its upgraded divertor manipulator (DIM-II) [7]. We report our results for the poloidal net erosion and re-deposition profiles, compare the results to spectroscopically determined estimates for gross erosion, and present preliminary results from ERO simulations to model the outcomes of the experiment.

2. Experimental details

2.1. Marker probes

For the experiment, a full poloidal row of special probes were manufactured from fine-grained graphite and mounted on a target tile, made of bulk W. The target tile was then transferred into the AUG torus for plasma exposure using the DIM-II divertor manipulator. A photograph of the target tile after the experiment, with the probes installed, is shown in Figure 1(a). Also the approximate strike-point region is marked in the figure. A schematic drawing of a single probe can be seen in Figure 1(b): Each probe consisted of a 4-mm wide poloidal W marker (thickness ~20 nm), a shallow (depth 0.2 mm, width 4 mm), uncoated trench magnetically downstream of the W marker, and finally an inclined Mo marker (thickness ~20 nm, width 4 mm) toroidally next to the trench. With this configuration, promptly re-deposited W atoms at the bottom of the trench were protected from further plasma exposure and unnecessary leading edges could be avoided. In addition, the erosion profiles of Mo and W could be compared, even though the Mo marker was on average more shadowed from plasma than the W marker. The location of the target tile in the AUG divertor is shown in Figure 1(c).

2.2. Plasma experiment

The marker probes were exposed to identical, low-density/high-temperature L-mode plasmas (AUG shots #31238-31251) in the vicinity of the OSP region of AUG. The overall exposure time (flat-top phases of the discharges) was ~80 s, after which the probes were retracted from the vessel for surface analyses.

The average plasma parameters were: plasma current I_p=0.8MA, toroidal field B_t=−2.5T, electron density in the core n_e~2.0×10^{19}m^{-3}, and auxiliary heating power by ECRH (electron cyclotron resonance heating) P_{ECRH}=1.3MW. This way, the density around the OSP was relatively low (0.5-2.0×10^{19}m^{-3}) while the electron temperature was on average 20-40 eV. The poloidal profiles for n_e and T_e, measured by fixed Langmuir probes in the OSP region as a function of distance from the strike point position, can be seen in Figures 2(a) and (b). The highest values for n_e and T_e, up to 3.0×10^{19}m^{-3} and 90eV, respectively, around the OSP are questionable and additional measurements by other probes have set the upper limits to $n_{e,max}$=3.0×10^{19}m^{-3} and $T_{e,max}$=45eV.

2.3. Erosion and re-deposition measurements

Before and after the experiment, all the three markers on the probes were measured using Rutherford Backscattering Spectroscopy (RBS). We used 2.0-MeV $^4He^+$ ions in the analyses and detected the backscattered particles at a scattering angle of 165°. The diameter of the beam was ~1 mm. By fitting the recorded spectra with the SIMNRA program, the elemental composition and thickness of each marker layer were determined.

For direct estimation of gross erosion, we also measured the intensity of the WI line at 400.9 nm along several different lines of sight in the poloidal direction in front of the OSP. A typical poloidal emission profile, expressed in terms of photon flux per solid angle, of W atoms as a function of distance from

the strike-point position can be seen in Figure 2(c). Corresponding measurements of the NII line at 399.5nm were also made and they imply similar, strong emission profiles in the vicinity of the OSP. The role of impurities on erosion is thus significant.

3. Results

3.1. Net erosion and re-deposition of W

Closest to the strike point, the W markers have been eroded by 7-10 nm, while in the peripheral regions net erosion is 3-4 nm. This we notice from Figure 3(a) where the thickness of the W marker before and after plasma exposure is shown as a function of the poloidal *s* coordinate; this coordinate runs along the surfaces of the PFCs at the AUG divertor such that the end points of the target tile are at *s*=987mm and *s*=1202mm (see Figure 1(c)). By taking the exposure time of 80s into account, the net erosion rates are within the range 0.04-0.13 nm/s, which are consistent with the reported long-term data in [8].

An interesting feature are the strong net deposition "barriers" on both sides of the most strongly eroded region, around *s*=1040mm and *s*=1080-1120mm. These can be caused by a strong influx of W from the areas surrounding the probes or from the W walls of the main chamber but also by re-distribution of the eroded material in the poloidal direction. Namely, material eroded from the strike point can migrate in multiple erosion-re-deposition steps (so-called walking) towards the private plasma region [9], thus contributing to the distinct peak just below the OSP. On the other hand, particles may also be driven by the $E_{pol} \times B_{tor}$ drift towards larger values of the *s* coordinate. This is one possible contributor to the broad deposition peak above OSP. Yet another possibility is transport of W from the farthest corners of the target tile (*s*>1180mm) towards the strike point. In the far scrape-off layer, plasma is cold and sparse, thus ionization and subsequent deposition of the emitted particles takes place only closer to the OSP. However, the largest contribution seems to come from general deposition of atoms in regions close to the strike point. This is supported by the observation that in the region *s*=1070-1100mm also nitrogen and boron show distinctive deposition peaks. That leads to a conclusion that large deposition of material from other parts of the torus can overcompensate for erosion of PFCs in specific poloidal regions, albeit at the same time more impurities will be around to intensify erosion further.

For comparison, the erosion/deposition profile of the Mo marker is shown in Figure 3(b). Qualitatively it matches to that of W in Figure 3(a), but the deposition barriers are much less prominent and the OSP values for Mo erosion only 6-7 nm even though Mo is a lighter element than W, thus more susceptible to erosion by plasma. We can understand this by the absence of other Mo sources than the markers in the divertor region and the fact that the recessed Mo markers were exposed to relatively cold plasmas. Thus, only phenomena like walking and $E \times B$ drifting can re-distribute material poloidally.

The re-deposition of W on the bottom of the carbon trench is 4-5 nm close to the OSP and ~1-2 nm in the peripheral zone. Thus, the ratio of net and gross erosion on the tile is 0.60-0.70 and prompt re-deposition 30-40% of gross erosion. This can be seen in Figure 3(c) where the poloidal re-deposition profiles along the C and Mo markers are shown. Again, strong deposition on both sides of the OSP can be seen even though the height of the peaks diminishes from C to Mo marker. This gives additional support to the ideas of longer-range W transport from the main chamber as discussed above and brings along additional uncertainty to the calculated prompt re-deposition factors. Of course, it is possible that shadowing has not been sufficient but also the trench has been exposed to plasma.

3.2. Spectroscopic estimates for gross erosion

The gross erosion of W can be alternatively estimated by passive emission spectroscopy. Assuming that none of the eroded atoms escape from the plasma before their ionization, the flux of W atoms, Γ_W, from the surface can be obtained from the measured absolute photon flux per solid angle, Φ (expressed in photons m^{-2} sr^{-1} s^{-1}) of a certain spectral line (here that of WI at 400.9nm) as follows [10]:

$$\Gamma_{\mathrm{W}} = \Phi \times 4\pi \times t \times \frac{S}{XB}(T_e),$$

where 4π is the total solid angle and t=80s the overall flat-top time of the experiment. The factor S/XB depends on electron temperature according to the formula [10]

$$\frac{S}{XB}(T_{\mathrm{e}}) = 53.7\left(1 - 1.04e^{-T_e/22.1}\right),$$

where T_{e} is expressed in eV. Around the strike point, the electron temperature is 20-40eV (see figure 2(b) and the discussion in section 2.2) and the photon flux around 2.0-2.5×10^{16} photons m^{-2} sr^{-1} s^{-1} (figure 2(c)). This results in WI fluxes of Γ_{W}=0.7-1.1×10^{21} atoms/m^2. Converted into uniform gross erosion of the coatings, we obtain 11-18nm, which is in line with the results we obtained in section 3.1, i.e., 11-15nm (sum of measured net erosion and re-deposition).

The peak in Figure 2(c) just above the OSP may be connected with the main-chamber flow of W atoms, as discussed in section 3.1. In the peripheral region (where the temperature is low, around 10 eV, and the photon flux <1.0×10^{16} photons m^{-2} sr^{-1} s^{-1}), the WI flux is <0.2×10^{21} atoms/m^2, corresponding to gross erosion of <3nm while *post mortem* data gives an estimate of 5-6nm. The spectroscopically obtained poloidal gross erosion profile is thus much sharper than the *post mortem* one, which motivates us to investigate the erosion/deposition behaviour in more detail using the ERO code.

3.3. First estimates of erosion and re-deposition by ERO

The experimental erosion and re-deposition profiles were modelled using the Monte Carlo code ERO [11]. We defined a simulation box that covered the entire toroidal extent of the marker tile (70mm) and had a size of 5mm in the poloidal direction. The third direction was defined perpendicular to the surface by 20mm. We assumed that the electron density and temperature were constant, which may not be valid near the OSP where significant gradients occur in the mm-scale. The first runs were carried out by varying T_{e} and n_{e} within intervals 10-40eV and 0.1-2.0×$10^{19}$$m^{-3}$, respectively, to estimate erosion and deposition on several different poloidal locations of the target tile (see Figure 2). At the bottom of the trenches, below the region defined by the magnetic field line (see Figure 1(b)), cold plasma was assumed (T_{e}=0.1eV, n_{e}=1.0×$10^{15}$$m^{-3}$). The simulation time was 2s at 0.01s steps; this was enough for equilibrium to be reached and, consequently, extrapolation to the total experimental time of 80s could be easily done. Periodic boundary conditions were also used such that none of the particles would escape the simulation box in the poloidal direction.

Examples of toroidal net erosion/deposition profiles of W and Mo in two different poloidal locations, corresponding to the cases close to the OSP (T_{e}=24eV, n_{e}=1.29×$10^{19}$$m^{-3}$) and at the far edge of the target tile (T_{e}=10eV, n_{e}=0.1×$10^{19}$$m^{-3}$) are shown in Figure 4. Close to the OSP (see Figure 4(a)), ERO predicts net erosion rate of 0.2-0.4nm/s for W (disregarding the edge effects between the interfaces of different markers) and ~0.6nm/s for Mo. These values are of the same order of magnitude but a factor of 2-10 higher as the post mortem results, 0.13nm/s for W and 0.09nm/s for Mo, indicated by dashed lines in the figure. In contrast, in the peripheral region (see Figure 4(b)) the situation is the opposite: ERO gives net erosion rates of 0.02nm/s for W and <0.005nm/s for Mo while the experimental values are ~0.05nm/s for both the materials. The qualitative picture was the same for re-deposition of W on C and Mo: strong overestimation, largely due to the periodic boundary conditions, around the OSP and clear underestimation further away. The absolute values scaled almost linearly with the density while increasing the electron temperature intensified erosion more abruptly. The ERO results for a relatively peaked net erosion profile suggest that poloidal transport has to be enabled and also the poloidal profiles of n_{e} and T_{e} have to be included in the model. Also, main chamber W sources and the role of impurities (particularly that of B and N) need to be considered; presently, neither of these is implemented in our simulation setup.

4. Conclusions

We have investigated net and gross erosion and prompt re-deposition of W in the OSP region of AUG with the help of marker tiles and their *post mortem* analyses. In the actual experiment the probes were exposed to low-density/high-temperature L-mode plasmas using the DIM-II divertor manipulator of AUG. The net erosion rates were determined to be 0.04-0.13nm/s, with the highest values observed closest to the OSP.

The re-deposition was some 30-40% of gross erosion, thus the ratio between net and gross erosion was 0.60-0.70 but significant uncertainties are connected with these estimates due to strong deposition peaks surrounding the most strongly eroded region. The re-deposition results are also different from earlier, spectroscopically determined data (typically prompt re-deposition ~50%). The discrepancy can be due to strong influx of W from the main chamber, which distorts the post mortem data from a situation with "pure" local erosion and re-deposition, or simply to the special plasmas used in our experiment. The role of main-chamber deposition was further evidenced by also nitrogen and boron showing deposition peaks in the region where the re-deposition "barriers" of W were observed and by the fact that re-deposition of Mo was much smaller than that of W. Future work include measuring also the profile of WII line (~364nm) for estimating prompt re-deposition directly by passive emission spectroscopy [10]. Also, more work is needed to judge whether shadowing has been enough in the experiment or whether the geometry has to be re-considered.

Spectroscopically, we studied also gross erosion by measuring the profile of the WI line at 400.9nm. Close to the OSP, the spectroscopy results agree with *post mortem* data while in the peripheral regions, erosion is clearly underestimated. The ERO simulations have so far been able to give correct order-of-magnitude estimates for net erosion of W but to properly reproduce the poloidal profiles requires modifying our setup, by including poloidal profiles of n_e and T_e in the simulations as well as poloidal transport of W along the target tile and by taking main-chamber sources and plasma impurities into account.

Acknowledgments

This work has been carried out within the framework of the EUROfusion Consortium and has received funding from the Euratom research and training programme 2014-2018 under grant agreement No 633053 and from Tekes – the Finnish Funding Agency for Innovation under the FinnFusion Consortium. The views and opinions expressed herein do not necessarily reflect those of the European Commission. We also acknowledge the contributions of the EUROfusion MST1 team.

References

[1] Pitts R A *et al* 2005 *Plasma Phys. Control. Fusion* **47** B303
[2] Roth J *et al* 2008 *Plasma Phys. Control. Fusion* **50** 103001
[3] Philipps V 2011 *J. Nucl. Mater.*, **415** S2
[4] Naujoks D *et al* 1996 *Nucl. Fusion* **36** 671
[5] Neu R *et al* 2011 *Plasma Phys. Control. Fusion* **53** 124040
[6] Brezinsek S and JET-EFDA contributors 2015 *J. Nucl. Mater.* doi: 10.016/j.nucmat.2014.12.007
[7] Herrmann A *et al* 2015 *Fus. Eng. Des.* doi:10.1016/j.fusengdes.2015.02.007
[8] Hakola A *et al.* 2014 *Phys. Scr.* **T159** 014027
[9] Strachan J D *et al* 2008 *Nucl. Fusion* **48** 105002
[10] van Rooij G J *et al* 2013 *J. Nucl. Mater.* **438** S42
[11] Kirschner A *et al* 2000 *Nucl. Fusion* **40** 989

Figure captions

Figure 1. (a) Photograph of the target tile after the plasma experiment with the marker probes installed. The approximate location of the strike-point region (grey area) and the direction of the magnetic field are also marked. (b) Schematic drawing of a single marker probe and its geometry. (c) Poloidal cross-section of the divertor of AUG and the location of the target tile during the experiment.

Figure 2. (a,b) Poloidal profiles of (a) electron density, n_e and (b) electron temperature, T_e, measured by fixed Langmuir probes in the OSP region. (c) Poloidal profile of the photon flux per solid angle of W atoms for the WI line at 400.9nm. In all the graphs, the grey zone marks the same strike-point region as that in Figure 1(a).

Figure 3. (a,b) Poloidal thickness profiles of the (a) W and (b) Mo markers before and after plasma exposure. The error bars are approximately 5%, mainly caused by inaccuracies in fitting of the RBS spectra. (c) Thickness of the W layer formed on the C trench and on the Mo marker after the plasma experiment. In all the graphs, the grey zone marks the same strike-point region as that in Figure 1(a).

Figure 4. ERO results for the toroidal net erosion/deposition profiles (in nm/s) of the W and Mo markers (a) close to the OSP (T_e=24eV, n_e=1.29×10^{19}m^{-3}) and (b) at the far edge of the target tile (T_e=10eV, n_e=0.1×10^{19}m^{-3}). Here, negative values mean net erosion, positive values net deposition. The dashed lines denote corresponding experimental values, extracted from the data in Figures 3(a) and (b).

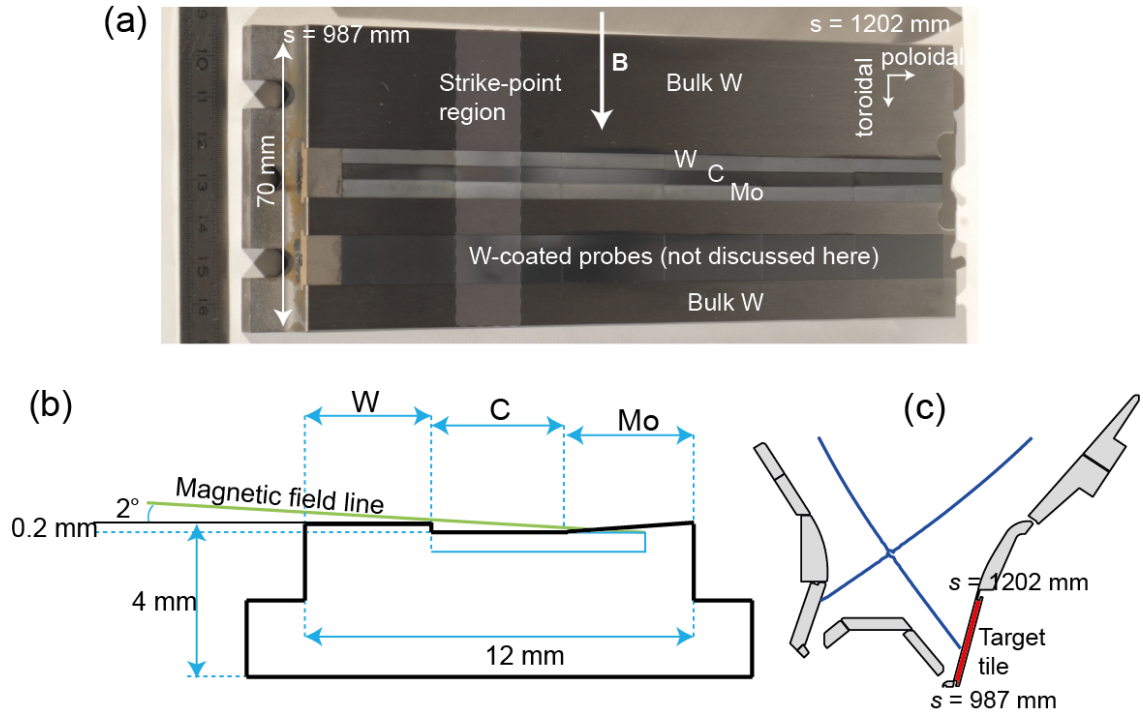
(a)
s = 987 mm
s = 1202 mm
B
Strike-point region
Bulk W
toroidal
poloidal
70 mm
W
C
Mo
W-coated probes (not discussed here)
Bulk W
(b)
W
C
Mo
2°
Magnetic field line
0.2 mm
4 mm
12 mm
(c)
s = 1202 mm
Target tile
s = 987 mm

Figure 1

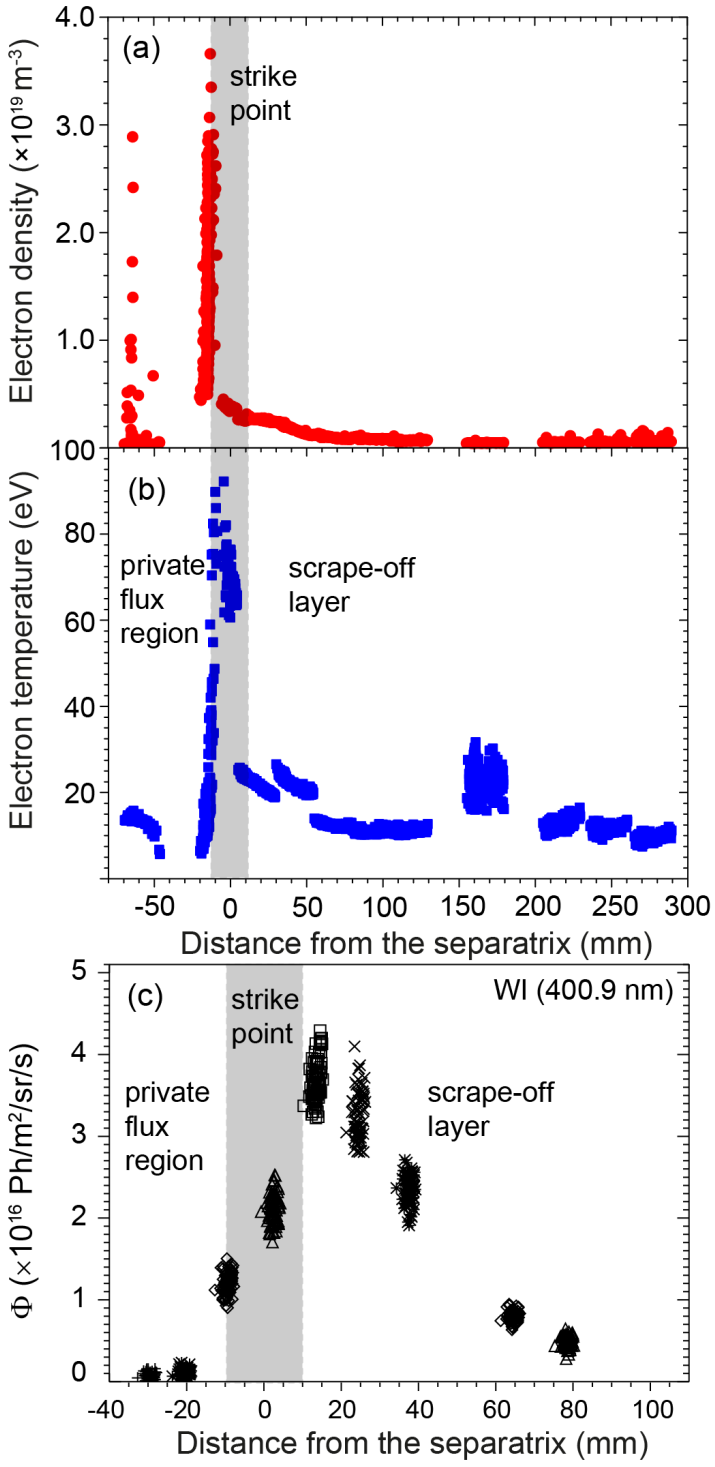
(a)
strike
point
Electron density (×10¹⁹ m⁻³)
4.0
3.0
2.0
1.0
(b)
private
flux
region
scrape-off
layer
Electron temperature (eV)
100
80
60
40
20
-50
0
50
100
150
200
250
300
Distance from the separatrix (mm)
(c)
strike
point
WI (400.9 nm)
private
flux
region
scrape-off
layer
Φ (×10¹⁶ Ph/m²/sr/s)
5
4
3
2
1
0
-40
-20
0
20
40
60
80
100
Distance from the separatrix (mm)

Figure 2

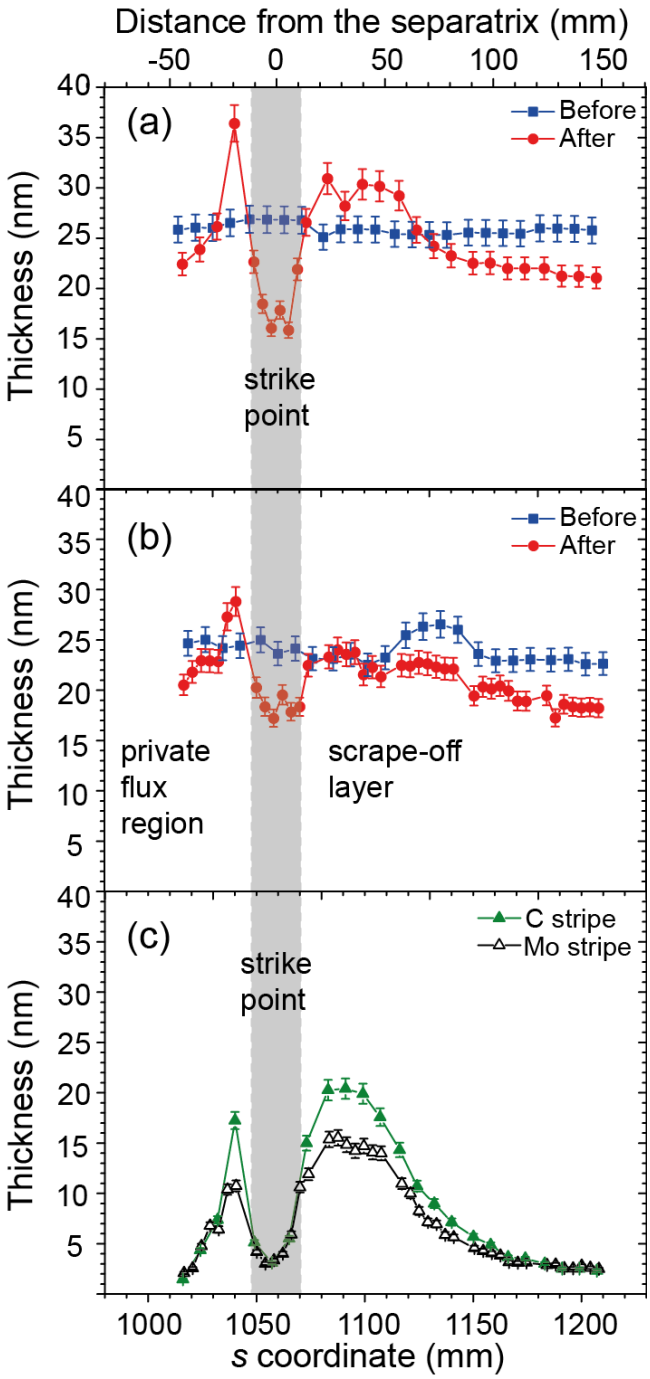
Distance from the separatrix (mm)
-50
0
50
100
150
(a)
Before
After
strike
point
Thickness (nm)
(b)
Before
After
private
flux
region
scrape-off
layer
(c)
C stripe
Mo stripe
strike
point
1000
1050
1100
1150
1200
s coordinate (mm)

Figure 3

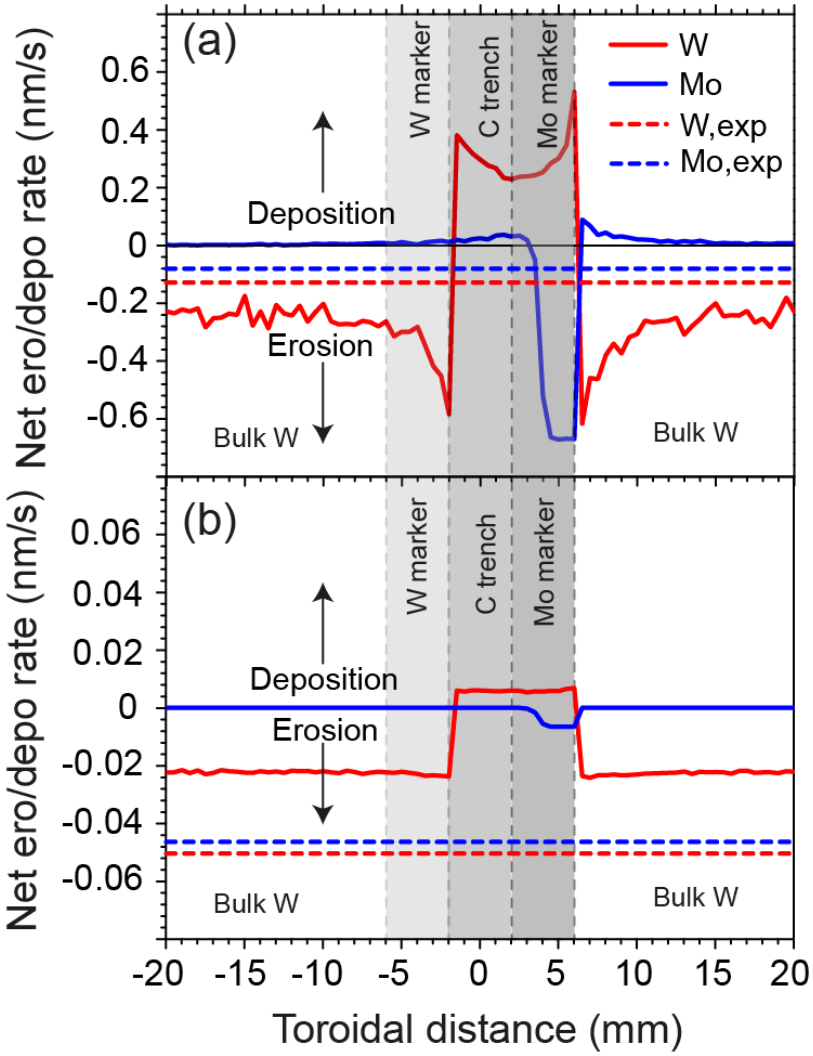
(a)
W marker
C trench
Mo marker
W
Mo
W,exp
Mo,exp
Deposition
Erosion
Bulk W
Bulk W
Net ero/depo rate (nm/s)
0.6
0.4
0.2
0
-0.2
-0.4
-0.6
(b)
W marker
C trench
Mo marker
Deposition
Erosion
Bulk W
Bulk W
Net ero/depo rate (nm/s)
0.06
0.04
0.02
0
-0.02
-0.04
-0.06
-20
-15
-10
-5
0
5
10
15
20
Toroidal distance (mm)

Figure 4